JOURNAL OF APPLIED PHYSICS **98**, 023903 (2005)

Magnetic switching of ferromagnetic thin films under thermal perturbation

Di Liu[a)]
Courant Institute of Mathematical Sciences, New York University, 251 Mercer Street, New York, New York 10012

Carlos Garcia-Cervera[b)]
Mathematics Department, University of California, Santa Barbara, California 93106

(Received 12 January 2005; accepted 3 June 2005; published online 21 July 2005)

In this paper, we study the magnetic switching of submicron-sized ferromagnetic thin films under thermal noise and external field. It is shown that the presence of the noise makes the switching easier with weaker external fields and induces more intermediate metastable states in the switching pathways. Different switching pathways are preferred at different temperatures. A quantitative relation between the temperature and the switching field for different metastable states is given through an adjusted Arrhenius formula near the critical field. Based on this, preferred switching pathways at different temperatures are obtained by comparing the energy barriers along different pathways. © *2005 American Institute of Physics*. [DOI: 10.1063/1.1988971]

I. INTRODUCTION

The process of magnetic switching of nanoscale ferromagnetic materials is a very important subject in the study of the magnetic recording process. Applications include technologies of manufacturing computer disks and memory cells, such as magnetoresistive random access memory (MRAM).[1,2] As the size of the magnetic devices decreases, thermal fluctuations become significant and must be included in realistic analysis and simulations. An attempt to incorporate thermal effects in micromagnetics was done by Brown, Jr. in (Ref. 3) for the special case of single-domain particles which have uniform magnetization. In Refs. 4 and 5, the hysteresis loops of single-domain particles at finite temperature were studied with large deviation theory. For more general cases, experiments and numerical simulations have been extensively carried on to understand the mechanism of the process (see Refs. 6–8 and the references therein) and various observations have been obtained. On the other hand, the magnetic switching under external field is known to be very nonlinear and hysteretic. So what is obviously of interest is the switching of magnetic field under the influences of both thermal perturbation and external field. Problems under investigation are the switching fields and the switching pathways at finite temperature in the hysteresis loops.

The paper is organized as follows. In Sec. II, we will show the thermal effects on the hysteresis loops of ferromagnetic thin films by solving the full stochastic Landau-Lifshitz (SLL) equation. It is observed that under thermal noise, the magnetization switches in the hysteresis loops with weaker external fields than without the noise. The noise may induce more intermediate stages in the switching pathways by driving the process into adjacent metastable states. And at different temperatures, the switching follows different pathways. Next, in Sec. III, we will analyze the overdamped SLL equation for single-domain particles and give a quantitative relation between the strength of the noise and the switching field for different metastable states using an adjusted Arrhenius formula near the critical field. We will also show that the system can be approximated by a reduced discrete Markov chain switching between metastable states. Finally, in Sec. IV, we will apply the same method developed in Sec. III to ferromagnetic thin films to predict the switching field between different metastable states in the hysteresis loops at finite temperature and give the preferred pathways at different temperatures. This is done by using the zero-temperature string method for micromagnetics to find the energy barriers between different metastable states.

II. MICROMAGNETICS UNDER THERMAL NOISE

A. Dynamics and numerical schemes

Based on the Landau-Lifshitz theory, the dynamics of the magnetization distribution in a ferromagnetic material is described by the following Landau-Lifshitz equation:

$$\dot{M} = -\gamma M \times H - \frac{\gamma\alpha}{\mathbb{M}_s} M \times (M \times H), \qquad (1)$$

where $|M| = \mathbb{M}_s(\text{const})$ is the saturation magnetization far from the Curie temperature. α is a dimensionless damping coefficient. $\gamma = ge/(2m_e)$ is the gyromagnetic ratio where e and m_e are the positive charge and mass of the electron. H is the local field computed as the following unconstrained first variation:

$$H = -\frac{\delta F}{\delta M}, \qquad (2)$$

where F is the Landau-Lifshitz energy functional,

[a)]Electronic mail: dliu@alumni.princeton.edu
[b)]Electronic mail: cgarcia@math.ucsb.edu

$$F[M] = \frac{1}{2}\int_{\Omega}\left\{\frac{C_{\text{ex}}}{\mathbb{M}_s^2}|\nabla M|^2 + \Phi\left(\frac{M}{\mathbb{M}_s}\right) - 2\mu_0 H_e M + \mu_0|\nabla U|^2\right\}dx. \tag{3}$$

Ω is the volume occupied by the material. C_{ex} is the exchange constant, and $\Phi(M/\mathbb{M}_s)=K_u(M_2^2+M_3^2)/\mathbb{M}_s^2$ is the anisotropy. $-2\mu_0 H_e M$ is the energy due to the external field H_e where μ_0 is the permeability of vacuum. The last term in the energy is due to the field induced by the magnetization inside the material such that

$$\Delta U = \begin{cases} \nabla M, & x \in \Omega \\ 0, & x \in \Omega^c, \end{cases} \tag{4}$$

together with the jump condition at the boundary $[U]=0$, $[\nabla U \cdot \nu]=-M\cdot\nu$.

To introduce the thermal effects, we replace H in (1) with $H+\sqrt{\kappa}\mathring{w}$ where w is a space-time white noise and $\circ$ denotes the Stratonovich integral in time. By the fluctuation-dissipation theorem, the strength of the noise should satisfy

$$\kappa = \frac{2\alpha K_B T}{(1+\alpha^2)\gamma\mathbb{M}_s}, \tag{5}$$

where K_B is the Boltzmann constant and T is the temperature. Then Eq. (1) becomes the SLL equation,

$$\dot{M} = -\gamma\times M(H+\sqrt{\kappa}\mathring{w}) - \frac{\gamma\alpha}{\mathbb{M}_s}M\times M\times(H+\sqrt{\kappa}\mathring{w}). \tag{6}$$

It is shown in Appendix A that the strength of the noise we add as in (5) is consistent with the case when the thin-film sample is reduced to single-domain particles,[3] for which both the magnetization and stray field are uniform: therefore, the exchange energy vanishes. This happens when the size of the material sample is very small.[9] We apply a quasistatic external field such that

$$H_e = (-1+\gamma\lfloor t/\Delta\rfloor\Delta)H_{\max}, \quad t\in\left[0,\frac{2}{\gamma}\right], \tag{7}$$

where Δ is the time interval during which each external field is applied. We use $\lfloor x\rfloor$ to denote the biggest integer no larger than x so the external field applied as above is changed quasistatically with a constant value on each subinterval $[k\Delta,(k+1)\Delta)$. $\gamma>0$ measures the speed with which the external field is changed.

We solve the Landau-Lifshitz equation [Eq. (1)] with an Euler-projection scheme. The Euler method is adopted for the time discretization and the magnetic field is renormalized to the sphere of constant magnetization at each time step:

$$M^* = M_{t_i} + \Delta t\left(-\gamma M_{t_i}\times H_{t_i} - \frac{\gamma\alpha}{\mathbb{M}_s}M_{t_i}\times M_{t_i}\times H_{t_i}\right),$$

$$M_{t_{i+1}} = \mathbb{M}_s\frac{M^*}{|M^*|}. \tag{8}$$

For the space discretization, we divide the computational domain into cells. In each cell we approximate the magnetization by a vector with constant magnitude, but free to rotate in any direction. We approximate the stray field by its average value in each cell. This stray field is computed using fast Fourier transform (FFT). The details of this computation can be found in (Ref. 10). We also solve the stochastic Landau-Lifshitz equation [Eq. (6)] with the Euler-projection scheme:

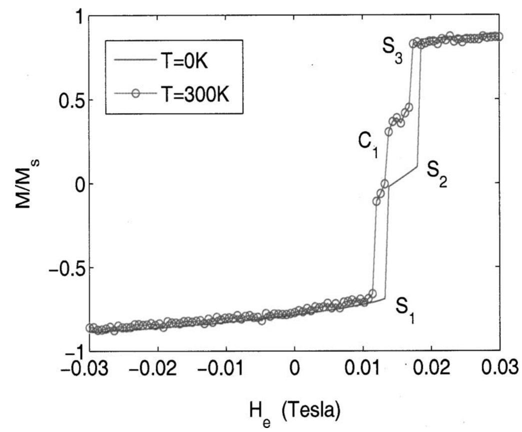

FIG. 1. Hysteresis loops of thin film at $T=0$ K and $T=300$ K.

$$M^* = M_{t_i} + \Delta t\left(-\gamma M_{t_i}\times \tilde{H}_{t_i} - \frac{\gamma\alpha}{\mathbb{M}_s}M_{t_i}\times M_{t_i}\times \tilde{H}_{t_i}\right),$$

$$M_{t_{i+1}} = \mathbb{M}_s\frac{M^*}{|M^*|}, \tag{9}$$

where

$$\tilde{H}_{t_i} = H_{t_i} + \sqrt{\kappa/\nu}\Delta w_{t_i}, \tag{10}$$

with ν being the volume of the computational cell. The time discretization for the thermal noise is performed in the following Stratonovich sense:

$$\Delta w_{t_i} = \frac{w_{t_{i+1}} - w_{t_{i-1}}}{\sqrt{2}}, \tag{11}$$

where $\{w_{t_i}\}$'s are independent and identically distributed standard random walks on the real line.

We choose the sample to be a $200\times200\times10\ \text{nm}^3$ square permalloy film and the computational grid to be 64×64. The time step is chosen to be 10^{-13} s for both the Landau-Lifshitz equation [Eq. (1)] and the stochastic Landau-Lifshitz equation [Eq. (6)]. We use the same physical parameters as in Ref. 7 such that

$$\alpha = 1,$$

$$\mu_0 = 4\pi\times10^{-7}\ \text{N/A}^2, \quad \gamma = 1.76\times10^{11}\ \text{T}^{-1}\text{s}^{-1},$$

$$\mathbb{M}_s = 9.0\times10^5\ \text{A/m}, \quad K_u = 1.0\times10^2\ \text{J/m}^3,$$

$$C_{\text{ex}} = 1.3\times10^{-11}\ \text{J/m}, \quad K_B = 1.380\,65\times10^{-23}\ \text{J/K}. \tag{12}$$

The external field is changed along the direction $(\cos\theta_0, \sin\theta_0, 0)$, $(0<\theta_0\ll1)$ from $-H_{\max}=-300$ Oe to $H_{\max}=300$ Oe. For the loop without noise, we initialize the magnetization uniformly with $(-1, 0, 0)$ in the loop. Each exter-

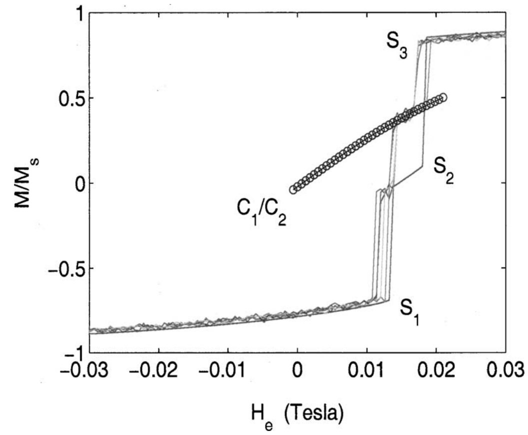

FIG. 2. Hysteresis loops of thin film for different realizations of the noise at $T=300$ K.

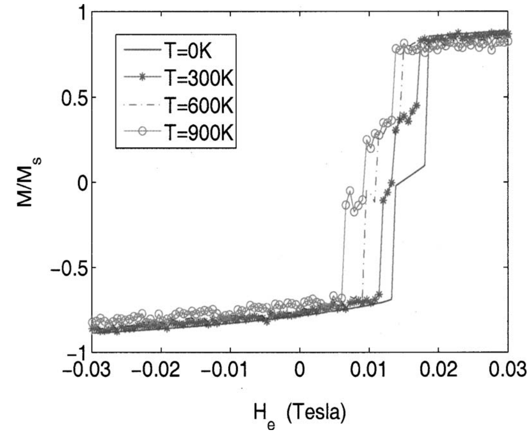

FIG. 4. Hysteresis loops of thin film at different temperatures.

nal field is run until the process reaches a stable state. This is guaranteed by small thresholds for the magnitudes of the gradient field $\delta F/\delta M$ and the relative changes of F and M. For the loop with noise, we initialize the magnetization with the stable state for the initial external field obtained in the loop without the noise. For each external field, the stochastic Landau-Lifshitz dynamics is run for 5 ns.

B. Hysteresis loops at zero and finite temperature

For ferromagnetic thin films, there are two stable configurations at zero temperature, commonly known as S state and C state. For S states, the magnetization in two end domains is parallel to each other and the magnetization forms an S-shape configuration. For C states, the magnetization in two end domains is opposite to each other and the magnetization forms a C-shape configuration.[11] In Fig. 1, we show the hysteresis loops without and with the thermal noise at temperature $T=300$ K. The switching in the zero-temperature loop has two phases. The first one is from S stage S_1 to S stage S_2 and the second one is from S stage S_2 to another S stage S_3. At finite temperature, there are two thermal effects on the loop. First, the switching occurs at a lower field in the $S_1 \rightarrow S_2$ switching. Second, with the noise, the magnetization switches along the $S_2 \rightarrow C_1 \rightarrow S_3$ pathway, with one more intermediate C state stage C_1. We apply decreasing/increasing external fields on stage C_1 without noise and get the stable states at zero temperature, which is shown in Fig. 2.

In Fig. 2, we also show the loops for different realizations of the thermal noise at the same temperature $T=300$ K. It can be seen that the thermal effect that the magnetization switches with a weaker field does not change with respect to realizations. But instead of switching to C_1, for some realizations with the same probability, the magnetization switches to another different C state stage C_2. For each external field, states in C_1 and C_2 stages have the same mean magnetization. Figure 3 gives the S state in stage S_2 and the C states in stages C_1 and C_2. It can be seen that there is a symmetry between C_1 and C_2 with respect to S_2. The magnetization in the top domains of S_2 and C_1 are opposite and the magnetization in the bottom domains of S_2 and C_1 are parallel. Meanwhile, the magnetization in the bottom domains of S_2 and C_2 are opposite and the magnetization in the top domains of S_2 and C_2 are parallel. In other words, from S_2, the magnetization switches to C_1 if the top domain of S_2 changes the direction and switches to C_2 if the bottom domain of S_2 changes the direction. For very few realizations, the intermediate C states are not observed. The same observation holds for temperatures up to $T=900$ K. We give in Fig. 4 the loops from 0 to 900 K. It can be seen that the higher the temperature, the weaker the external field needed for the $S_1 \rightarrow S_2$ switching is.

Now we raise the temperature up to $T=1200$ K to see the thermal effect on the hysteresis loops at higher temperatures. In Fig. 5, we show some realizations of the loops at $T=1200$ K in which the switching follows the $S_2 \rightarrow C_1/C_2 \rightarrow S_3$ pathways. Consistent with the above observations, the $S_1 \rightarrow S_2$ switching happens at much lower fields. The only difference from the lower temperatures is that after the magnetization settles at the S_3 stage, it may switch to another C state which has a mean magnetization close to that of the S_3 states. Figure 6 shows a different switching pattern for other realizations at $T=1200$ K. The magnetization first switches

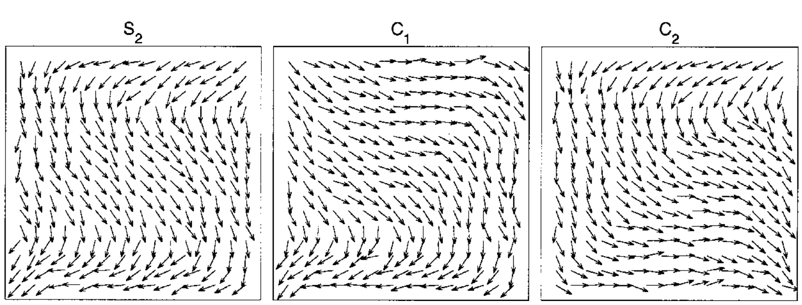

FIG. 3. S state in stage S_2 and C states in stage C_1 and C_2.

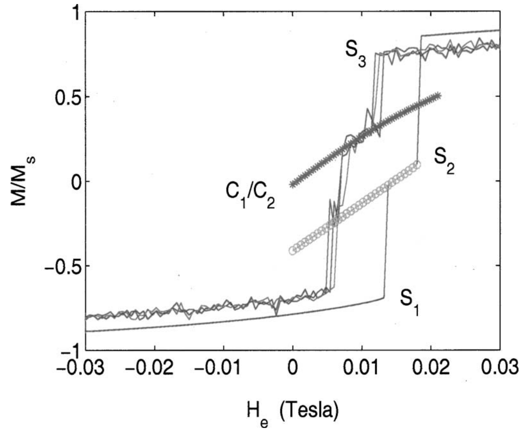

FIG. 5. Hysteresis loops at $T=1200$ K following the $S_2 \to C_1/C_2 \to S_3$ pathways.

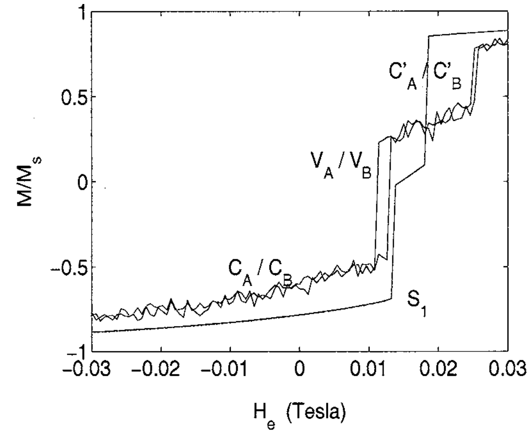

FIG. 6. Hysteresis loops at $T=1200$ K following the vortex pathways.

at a negative external field to a C state. There are two different configurations for this C state, which we denote by C_A and C_B. Then at a positive external field, the magnetic field switches to a vortex state V_A or V_B, whose configuration depends on the previous C state. After the vortex state, the magnetization will switch to another C state stage C_A' or C_B' depending on the path it has followed. Again, after the C_A'/C_B' stages, the magnetization may switch to another C or S state with a close mean magnetization. In short, for these realizations, the switching follows the $S_1 \to C_A \to V_A \to C_A'$ or $S_1 \to C_B \to V_B \to C_B'$ pathway. Figures 7 and 8 give the states in these pathways. The observation that the switching between C states is through vortex nucleation and propagation is consistent with Ref. 8.

In conclusion, the above results show that the thermal noise makes the magnetic switching easier with weaker external fields and induces different switching pathways. The higher the temperature, the more different pathways the switching may follow. A quantitative study will be given in subsequent sections.

III. MAGNETIC SWITCHING OF SINGLE-DOMAIN PARTICLES

In this section, we want to give quantitatively the relation between the strength of thermal noise and the switching field for different metastable states in the hysteresis loops of single-domain particles in which the magnetization is uniform. This relation is given through Eq. (22). If $\alpha \gg 1$, the first term (the gyromagnetic term) on the right-hand side of the Landau-Lifshitz equation [Eq. (1)] is dominated by the second term (the damping term) and hence can be dropped. Transforming into angular variables and introducing the thermal noise, we get the following random perturbed gradient system describing the overdamped Landau-Lifshitz dynamics for single-domain particles under thermal noise and changing external field:

$$\dot{\phi} = -\frac{1}{\delta}\nabla_\phi V(\phi,t) + \sqrt{\frac{2\epsilon}{\delta}}\dot{w}, \tag{13}$$

where

$$V(\phi,t) = -\tfrac{1}{4}\cos 2(\phi-\theta_0) - h_0(-1+\lfloor t/\Delta \rfloor \Delta)\cos\phi. \tag{14}$$

Here ϕ represents the angle between the magnetization and the external field. δ is a constant obtained from variable transformation and depends on the physical parameters of the system. ϵ is the strength of the noise determined by fluctuation-dissipation theorem and w is a standard Brownian motion. The energy function $V(\phi,t)$ is chosen to be the Stoner-Wohlfarth potential for single-domain ferromagnetic materials. It is a special case of the Landau-Lifshitz potential when the magnetization is uniform across the sample. We are assuming no crystalline anisotropy here for simplicity and the fact that it is usually smaller than the shape anisotropy in permalloy. The first term of $V(\phi,t)$ is the anisotropy and the second is the energy due to the following time-dependent external field:

$$h = h_0(-1+\lfloor t/\Delta \rfloor \Delta), \quad t \in [0,2], \tag{15}$$

which is changed from $-h_0$ to h_0. Δ represents the observation time for each external field. $\lfloor x \rfloor$ is defined as before to be the biggest integer no larger than x. Notice that we can also write $V=V_h(\phi)$. θ_0 gives the preferred direction of magneti-

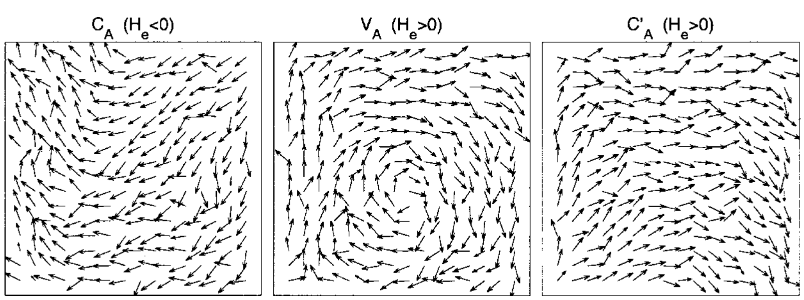

FIG. 7. C and vortex states in $C_A \to V_A \to C_A'$ pathway with increasing H_e.

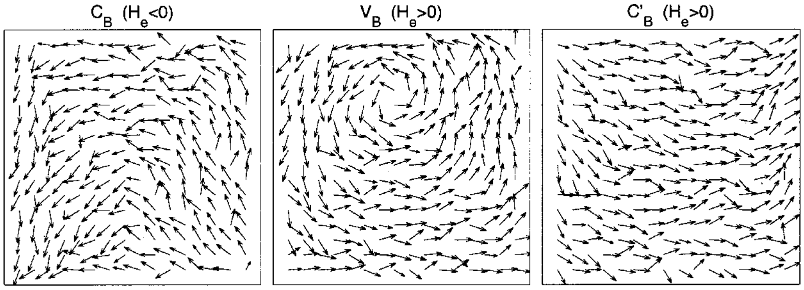

FIG. 8. C and vortex states in $C_B \rightarrow V_B \rightarrow C'_B$ pathway with increasing H_e.

zation by the sample. For simplicity and numerical tractability, we choose the parameters such that

$$(\delta, h_0, \Delta, \theta_0) = (2.0 \times 10^{-5}, \pm 1, 2.0 \times 10^{-3}, \pi/10). \tag{16}$$

There are several time scales in system (13). The first one is the relaxation time scale for the process to reach the steady states of $V_h(\phi)$. The second, represented by Δ, is the observation time scale for each external field. The third one is the exit time scale which is the waiting time for the process to switch from one steady state of $V_h(\phi)$ to another driven by the noise. This time scale depends on ϵ, the strength of the noise. The fourth time scale is the switching time scale for the execution of the switching. By choosing

$$\delta \ll \Delta, \quad \epsilon \ll 1, \tag{17}$$

we have the relaxation and switching time scales much smaller than the other two. Hence we discuss the behavior of the system when the observation time scale and exit time scale change with Δ and ϵ to study the effect of the thermal perturbation on the hysteresis loops. For $\epsilon=0$ and $\epsilon=0.0025$ [Fig. 9], plotting $\cos\phi(h)$ against h when $h_0=\pm 1$ gives the hysteresis loops generated by the separation of the local minima of $V_h(\phi)$. The loops under noise are the numerical solutions of $\mathbb{E}\cos[\phi(t)]$ obtained by first solving the forward Fokker-Planck equation for the probability distribution of $\phi(t)$ with periodic boundary conditions, then taking the numerical integration for $\phi(t)$ with respect to the solution of the Fokker-Planck equation. It can be seen that the noise makes the switching easier with a weaker external field.

Now we want to analyze the relation between the switching field and (Δ, ϵ). $V_h(\phi)$ can be numerically computed very easily. First, we have the observation that function $V_h(\phi)$ exhibits different properties for different h. Letting

$$h_c = 0.590, \tag{18}$$

which is the switching field in the hysteresis loop without noise, we have the following:

(1) for $h \leqslant -h_c$ and $h \geqslant h_c$, $V_h(\phi)$ has one minimum and one maximum, and
(2) for $-h_c < h < h_c$, $V_h(\phi)$ has two local minima and two local maxima.

The energy landscapes of V for different values of h are shown in Fig. 10. Due to symmetry, we only analyze the switching near the critical field h_c when the external field is applied from -1 to 1. For $-h_c < h < h_c$, we denote by $\psi_1(h)$ the local minimum of $V_h(\phi)$ shown in Fig. 9 as the bottom loop without noise when h is changed from -1 to 1 and denote by $\psi_2(h)$ the other local minimum. We also denote by $\theta_1(h)$ and $\theta_2(h)$ the local maxima. Let $\theta(h) \in \{\theta_1(h), \theta_2(h)\}$ be the critical point with a lower-energy barrier such that $V_h[\theta(h)] = \min\{V_h[\theta_1(h)], V_h[\theta_2(h)]\}$. We define the energy barrier $\Delta V(h)$ from ψ_1 to ψ_2 to be

$$\Delta V(h) = V_h[\theta(h)] - V_h[\psi_1(h)]. \tag{19}$$

Numerical results given in Fig. 11 show that $\Delta V(h)$ is monotonically decreasing with respect to h on the interval $[-h_c, h_c]$.

Notice that on each time subinterval $[i\Delta, (i+1)\Delta)$, dynamics (13) is homogeneous, i.e., the coefficients are time

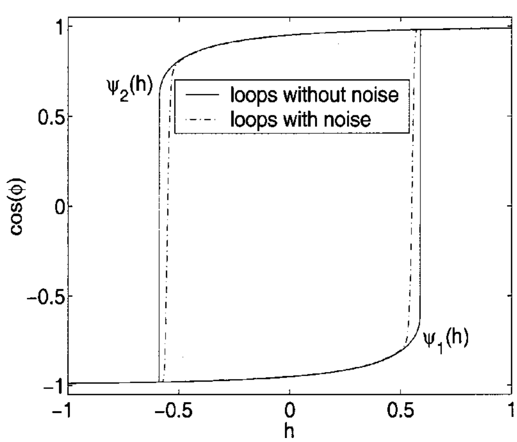

FIG. 9. Hysteresis loops of single-domain particle with and without the noise.

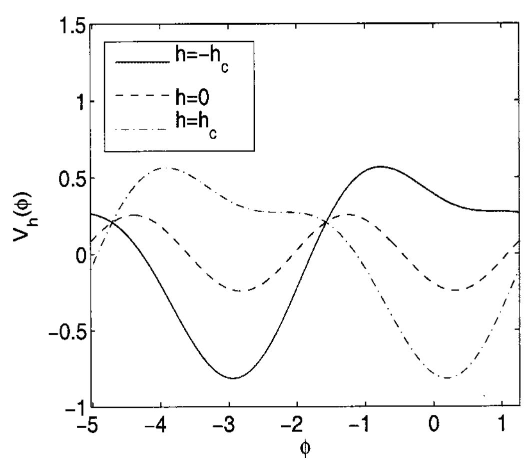

FIG. 10. Energy landscapes of the single-domain particles for different external fields.

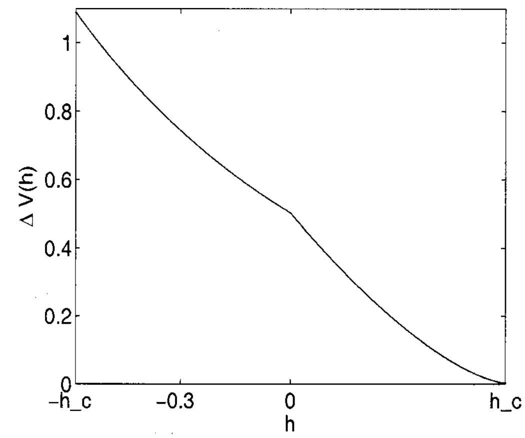

FIG. 11. The energy barrier $\Delta V(h)$ for $-h_c<h<h_c$.

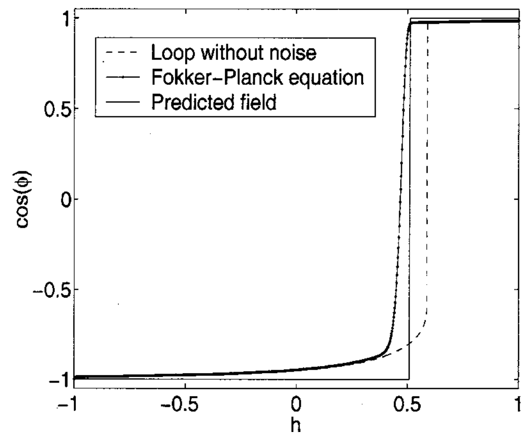

FIG. 12. Predicted switching field for single-domain particle when $\epsilon=0.01$.

independent. It is shown in Appendix B that for each external field near h_c, the mean exit time τ for the process to overcome the energy barrier ΔV to switch from ψ_1 to ψ_2 is given by the following adjusted Arrhenius formula:

$$\tau(h) = \frac{\nu_0 \delta}{\epsilon^{1/3}} \exp\left[\frac{\Delta V(h)}{\epsilon}\right], \tag{20}$$

where $\nu_0=\int_0^\infty e^{-x^3/6}dx^2/|V^{(3)}[\lim_{h\to h_c^-}\psi_1(h)]|^{2/3}$. Direct numerical computation shows that $\nu_0=2.127$. Due to the exponential dependence of the exit time scale τ on ΔV and the monotonicity of ΔV, the exit time scale decreases when h approaches h_c. The switching should be most probable when the exit time scale is comparable to the observation time scale such that

$$\tau(h^*) = \Delta. \tag{21}$$

The monotonicity of $\Delta V(h)$ implies an inverse function $(\Delta V)^{-1}$ for ΔV and a unique solution for Eq. (21). Then we have the following equation for the switching field in the hysteresis loops under random perturbation:

$$h^* = (\Delta V)^{-1}\left[\epsilon \ln\left(\frac{\epsilon^{1/3}\Delta}{\nu_0 \delta}\right)\right]. \tag{22}$$

We solve the Fokker-Planck equation to get the loops for different strengths of the noise and pick up the switching field in the loop to be the first field where the magnetization is fully switched. Table I gives this result and the switching field predicted by (22). The relative error is <0.03. The hysteresis loop and the predicted switching field when $\epsilon=0.01$ are shown in Fig. 12.

By the fact that the dynamics is homogeneous on each subinterval, we know[12] that for each external field, the nth($n \in \mathbb{N}$) moment $\tau^n(\phi)$ of the exit time satisfies the equation

TABLE I. Simulated and predicted switching fields of single-domain particles.

ϵ	0.00125	0.0025	0.005	0.01
Switching field	0.580	0.566	0.542	0.500
Predicted field	0.574	0.563	0.544	0.513

$$-\frac{1}{\delta}\frac{\partial V}{\partial \phi}\frac{\partial \tau^n}{\partial \phi} + \frac{\epsilon^2}{\delta}\frac{\partial^2 \tau^n}{\partial \phi^2} = -n\tau^{n-1}. \tag{23}$$

Boundary layer analysis as in Ref. 13 can show that except on a boundary layer of thickness of $n\epsilon^2$,

$$\tau^n(\phi) = (nK)\tau^{n-1}(\phi) = \text{const}. \tag{24}$$

This means that away from the boundary, the exit time can be approximated by an exponentially distributed random variable with parameter $\tau(\phi)=K$ in the sense that the moments are asymptotically close. Similar results are also given in Ref. 14 by a more subtle analysis. The above analysis implies that we can approximate dynamics (13) by a discrete Markov chain in which the process switches between $\psi_1(h)$ and $\psi_2(h)$ with exponentially distributed transition probabilities, which provides a method to dramatically reduce the computation by simulating the Markov chain instead of solving the Fokker-Planck equation. Figure 13 gives the expectations of the magnetization with respect to this Markov chain using the mean exit time τ given by (20) when $\epsilon=0.01$. It can be seen that it is almost identical with the result by solving the Fokker-Planck equation.

IV. SWITCHING OF FERROMAGNETIC THIN FILMS

From Sec. II, we see that the thermal noise has two effects on the magnetic switching. The first is to make the switching easier with weaker external fields. The second is to induce different switching pathways at different temperatures. The questions that need to be answered are what the switching field under noise is and which pathways are preferred at different temperatures. In this section, we will apply the adjusted Arrhenius formula [Eq. (20)] to these problems.

A. Energy landscapes under different external fields

First we want to study the energy landscapes of thin films under different external fields and the implications in magnetic switching. For a given energy function or functional $V(x)$, the minimum energy path (MEP) φ between different metastable states A and B is defined to be the curve connecting A and B and satisfying the following equation:[15]

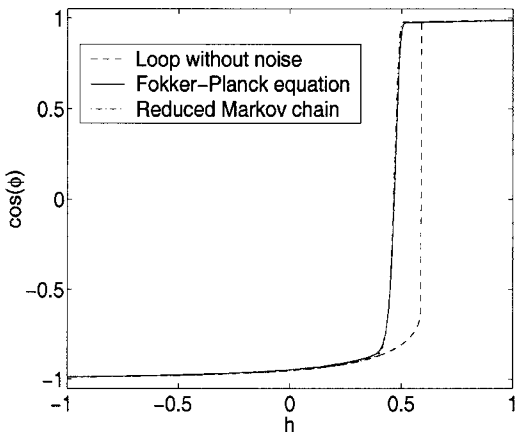

FIG. 13. Simulation of the hysteresis loop with the reduced Markov chain when $\epsilon=0.01$.

$$\nabla^{\perp} V(\varphi) = 0, \tag{25}$$

where $\perp$ denotes the projection onto the hyperplane perpendicular to φ. It it known[16] that, for Landau-Lifshitz potential and dynamics, the MEP shares the same critical points and hence the same energy barriers with the transition pathways between different metastable states at finite temperature. The zero-temperature string method for micromagnetics[16] solves the MEP by evolving the following gradient flow in the path space:

$$\phi_t = -\nabla^{\perp} V(\phi) + r\hat{t}, \tag{26}$$

where $\phi=\phi_{[0,1]}$ is a curve connecting A and B. $\hat{t}=\phi_\alpha/|\phi_\alpha|$ is the unit tangent along ϕ. r is a Lagrangian multiplier which keeps a certain parametrization of the evolving curve. In the following, we are going to choose r such that

$$|\phi|_\alpha/|\phi|_1 = \sin(\alpha^\eta \pi/2), \quad \alpha \in [0,1], \tag{27}$$

where $|\phi|_\alpha$ is the arclength of the evolving curve. $\eta>1$ is a fixed number. This parametrization allows to focus on the nucleation of the switchings. The string method can be easily parallelized by dividing the evolving curve into a certain number of subcurves, all evolving with (26). This can be implemented by an message passing interface (MPI) structure.

In Fig. 14, we give the energy barriers between S_1 and S_2 stages for different external fields obtained by using the string method. It can be seen that consistent with the case of single-domain particles, the energy barrier decreases when the external field is increased. This means that the higher the temperature, the lower the field needed for the switching, which is also observed in direct simulations.

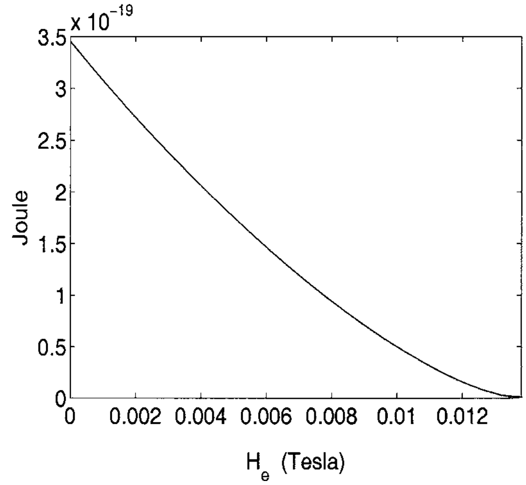

FIG. 14. The energy barriers between S_1 and S_2 stages for different external fields.

B. Switching field at finite temperature

Now we want to study the switching field in the hysteresis loops of thin films with the adjusted Arrhenius formula. We do the following substitution for (20) in the context of the stochastic Landau-Lifshitz dynamics:

$$\delta \to \frac{1}{\alpha\gamma\mathbb{M}_s}, \quad \epsilon \to k_B T. \tag{28}$$

Then we have the adjusted Arrhenius formula for ferromagnetic thin film which gives the mean exit time from the neighborhood of one metastable state near the critical field:

$$\tau = \frac{\nu_0}{\alpha\gamma\mathbb{M}_s(k_B T)^{1/3}} \exp[\Delta F/(k_B T)], \tag{29}$$

where ΔF is the energy barrier between different metastable states. ν_0 is a prefactor depending on the third-order curvature of the energy landscape at the critical field. In the hysteresis loops with thermal noise, the switching should happen when the exit time scale is equal to the observation time scale, i.e.,

$$\tau = \Delta. \tag{30}$$

Due to the difficulty arising from the infinite dimensional nature of the Landau-Lifshitz dynamics, we still do not have efficient tools to estimate ν_0. Since the dependence of τ on the energy barrier ΔF is exponential and much more significant than the dependence of τ on ν_0, we assume $\nu_0=1$. By the monotonicity of ΔF, we have the following equation for the switching field at temperature T:

$$H_e^* = (\Delta F)^{-1}\{k_B T \ln[\Delta\alpha\gamma\mathbb{M}_s(k_B T)^{1/3}]\}. \tag{31}$$

TABLE II. Simulated and predicted switching fields of thin films.

Temperature (K)	100	200	300	400	500	600
Mean switching field (Oe)	132.7	125.2	124.4	120.7	103.4	96.7
Predicted field (Oe)	127.1	121.2	116.3	111.7	107.5	103.5

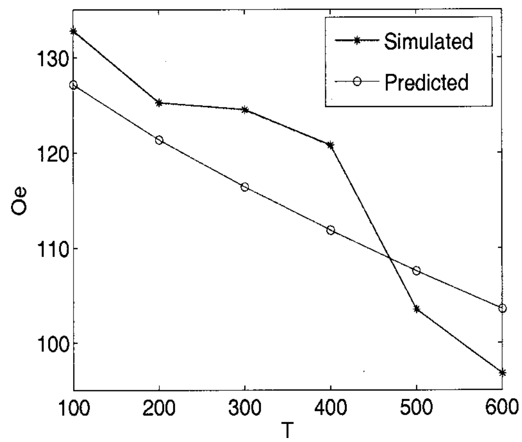

FIG. 15. Simulated and predicted switching field between S_1 and S_2 stages.

Now we focus on the $S_1 \rightarrow S_2$ switching. We use formula (31) to predict the switching field for temperatures from 100 to 600 K. At the same time, we compute eight realizations of the loops for each temperature and take the mean switching field. Table II and Fig. 15 give the mean switching fields and the predicted fields. The relative error is <0.08.

C. Preferred pathways at different temperatures

Now we want to study the preference of different pathways at different temperatures. We first focus on the lower temperatures. From the results in Sec. II, we know that at zero temperature, the switching follows the $S_2 \rightarrow S_3$ pathway while at finite temperature, the switching follows the $S_2 \rightarrow C_1/C_2 \rightarrow S_3$ pathways. Figure 16 gives the energy barriers of the $S_2 \rightarrow S_3$ and $S_2 \rightarrow C_1$ switchings for different external fields. Due to symmetry, the energy barriers for the $S_2 \rightarrow C_2$ switching will be the same as those for the $S_2 \rightarrow C_1$ switching. It can be seen that the energy barriers for the $S_2 \rightarrow C_1/C_2$ switchings are much smaller than the barriers of the $S_2 \rightarrow S_3$ switching. This means that the $S_2 \rightarrow C_1/C_2 \rightarrow S_3$ pathways are more preferred than the $S_2 \rightarrow S_3$ pathway. In

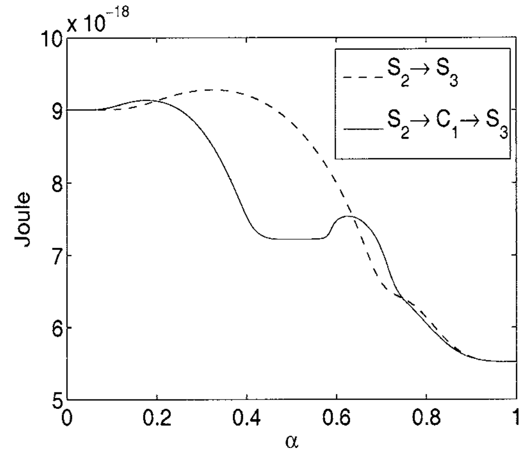

FIG. 17. Energy along the MEPs of $S_2 \rightarrow S_3$ and $S_2 \rightarrow C_1 \rightarrow S_3$ switchings when $H_e = 90$ Oe.

Fig. 17, we give the energy along the minimum-energy paths of $S_2 \rightarrow S_3$ and $S_2 \rightarrow C_1 \rightarrow S_3$ switchings when the external field is 90 Oe.

Now we move to the higher temperature of 1200 K. Figure 18 gives the energy barriers for the $S_1 \rightarrow C_A$ pathways for different external fields. Again for the reason of the symmetry between C_A and C_B with respect to S_1, the energy barriers for the $S_1 \rightarrow C_B$ is the same. It can be seen that the energy barrier increases when external field is increased from negative to positive. Since this switching is away from the critical field, we can use the original Arrhenius formula without the adjustment in the prefactor:

$$\tau = \frac{\nu_0}{\alpha\gamma\mathbb{M}_s} \exp[\Delta F/(k_B T)]. \tag{32}$$

Assuming $\nu_0 = 1$ again in switching condition (30) gives

$$H_e^* = (\Delta F)^{-1}[k_B T \ln(\Delta\alpha\gamma\mathbb{M}_s)]. \tag{33}$$

The predicted switching field for $S_1 \rightarrow C_A/C_B$ at $T=1200$ K using formula (33) is $H^*_{e,1200} = -129.1197$ Oe. At $T=600$ K, the predicted field is $H^*_{e,600} = -348.9502$ Oe. Notice that $H^*_{e,600} < -H_{\max} < H^*_{e,1200}$ where $H_{\max}$ is the maximum exter-

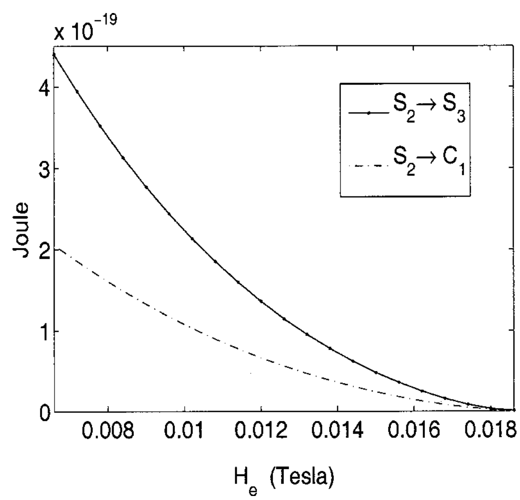

FIG. 16. Energy barriers of $S_2 \rightarrow S_3$ and $S_2 \rightarrow C_1$ switchings for different external fields.

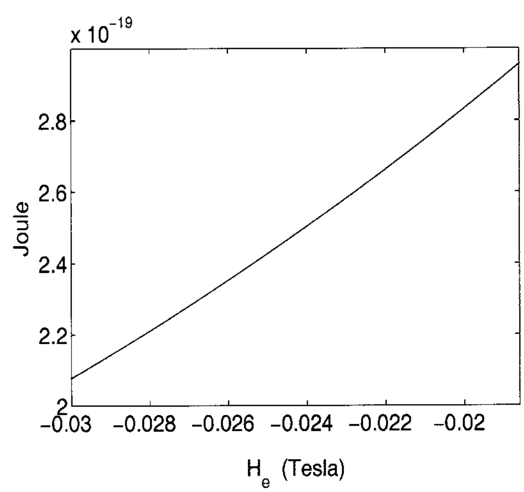

FIG. 18. Energy barriers for the $S_1 \rightarrow C_A$ switching under different external fields.

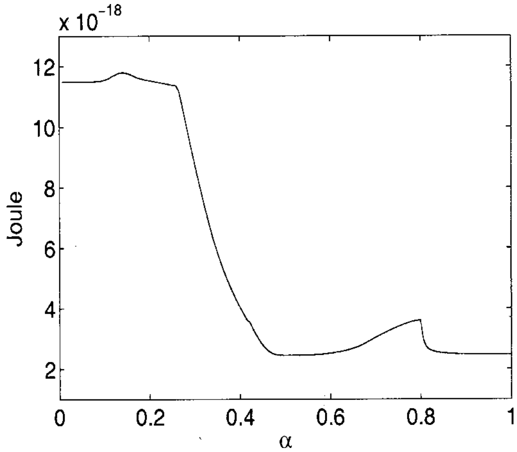

FIG. 19. Energy along the MEP of $C_A \rightarrow V_A \rightarrow C_A'$ switching when $H_e = 180$ Oe.

nal field applied on the sample. This means that, under the external field we are applying, the $S_1 \rightarrow C_A/C_B$ switching is impossible at $T=600$ K and is more preferred at $T=1200$ K. In other words, when the external field is negatively large and the temperature is high, the energy barriers separating S_1 and C_A/C_B are so small that they are ignored by the fluctuation. This also by symmetry explains the observation that the process may switch to other S and C states after C_A'/C_B' when the external field gets positively large and the fluctuation becomes important again. In Fig. 19, we give the energy along the minimum energy path along the $C_A \rightarrow V_A \rightarrow C_A'$ switching when the external field is 180 Oe. The increasing energy barrier also implies that the $S_1 \rightarrow C_A/C_B$ switching becomes difficult when the external field is increased from negative to positive. This is why for some of the realizations, when the $S_1 \rightarrow C_A/C_B$ switching does not happen at large negative external fields, the switching will follow the $S_1 \rightarrow S_2$ pathway later when the external field gets positive.

V. CONCLUSIONS

So far, we have studied the effects of incorporating thermal noise into the full Landau-Lifshitz dynamics for ferromagnetic thin films and the relation between the thermal noise and switching field in the hysteresis loops. The stochastic Landau-Lifshitz equation with Stratonovich noise is solved with an Euler-projection method. The energy barriers between different metastable states under different external fields are obtained with the string method. Hence the switching field can be predicted for different temperatures by the adjusted Arrhenius formula and preferred pathways at different temperatures can be given. Future work involves the asymptotics for the prefactor of the Arrhenius formula in infinite dimensions.

ACKNOWLEDGMENTS

We are grateful to Weinan E, Robert Kohn and Eric Vanden-Eijnden for stimulating discussions and insightful comments. One of the authors (D.L.) partially acknowledges partial support by NSF via Grant No. DMS97-29992 and by ONR via Grant No. N00014-01-1-0674. We want to thank Princeton Institute for Computational Science and Engineering for providing the computing resources.

APPENDIX A: THE STRENGTH OF THE THERMAL NOISE

Here we want to give an argument for the strength of the noise we added in the Landau-Lifshitz equation as given by (5). In Ref. 3, the following Gilbert equation was used to describe the dynamics of the magnetization for single-domain particles:

$$M_t = \gamma_0 M \times \left(-\frac{1}{\nu}\,\partial F/\partial M - \eta M_t\right) = \gamma_0 M(H - \eta M_t), \tag{A1}$$

where F is the Landau-Lifshitz potential and ν is the volume of the particle. Comparing the coefficients with (1) gives

$$\gamma_0 = -\gamma(\alpha^2+1), \quad \eta = \frac{\alpha}{\gamma \mathbb{M}_s(\alpha^2+1)}. \tag{A2}$$

To incorporate the thermal noise, in Ref. 3, the field H in (A1) was replaced by $H+\mathring{h}_t$ where $\mathring{h}_t$ is a Stratonovich noise white in time. It is shown[3] that for the above equation to have an equilibrium distribution $e^{-F(M)/(k_BT)}$, the strength of the noise h_t should satisfy the following:

$$\langle h_t^i \rangle = 0, \quad \langle h_t^i h_{t+\tau}^j \rangle = \frac{2k_BT\eta}{\nu}\delta(\tau) = \frac{2\alpha k_BT}{\gamma \mathbb{M}_s(\alpha^2+1)\nu}\delta(\tau)$$
$$= D\delta(\tau). \tag{A3}$$

If we add the noise in (6) such that $\kappa = 2\alpha k_BT/\gamma\mathbb{M}_s(\alpha^2+1)$. Then after space discretization, the noise on each computational cell k satisfies

$$\langle w_t^i \rangle = 0, \quad \langle w_t^i, w_{t+\tau}^j \rangle = D\delta_{ij}\delta(\tau), \tag{A4}$$

which is consistent with (A3) and fluctuation-dissipation theorem.

APPENDIX B: ADJUSTED ARRHENIUS FORMULA NEAR THE CRITICAL FIELD

In this Appendix, we want to give the adjusted Arrhenius formula for the single-domain particles near the critical field h_c. Notice that by the definition $V_h[\theta(h)] = \min\{V_h[\theta_1(h)], V_h[\theta_2(h)]\}$. With a much higher probability, the process switches by overcoming $\theta(h)$ and $\Delta V(h)$ instead of overcoming the other critical point $\{\theta_1, \theta_2\}/\theta$, which has a higher energy barrier. Hence we can impose a reflecting boundary condition at $\{\theta_1, \theta_2\}/\theta$. Solving directly [Eq. (23)] for $n=1$,[12] we have

$$\tau \approx \frac{\delta}{\epsilon}\int_{\psi_1}^{\psi_2} d\alpha \exp[V(\alpha)/\epsilon] \int_{\{\theta_1,\theta_2\}/\theta}^{\theta} d\beta \exp[-V(\beta)/\epsilon]. \tag{B1}$$

It can be seen that when $h \rightarrow h_c^-$, $\theta(h) \rightarrow \theta^*$ and $\psi_1(h) \rightarrow \theta^*$ for some θ^*. Notice that by the stability condition,

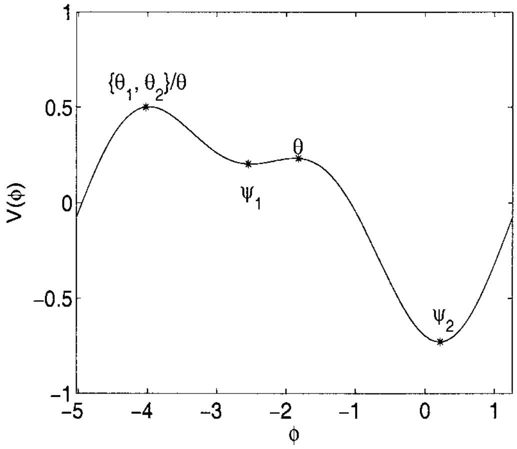

FIG. 20. Energy landscape for single-domain particle near the critical field.

$$V_h'[\theta(h)] = V_h'[\psi_1(h)] = 0, \quad V_h''[\theta(h)] \leqslant 0 \leqslant V_h''[\psi_1(h)]. \tag{B2}$$

By continuity, we have for $i=1, 2$,

$$V_h^{(i)}(\theta^*) = \lim_{h\to h_c^-} V_h^{(i)}[\theta(h)] = \lim_{h\to h_c^-} V_h^{(i)}[\psi_1(h)] = 0, \tag{B3}$$

while direct computation shows that $V^{(3)}(\theta^*) < 0$. We make the following third-order Taylor expansion for $\psi_1 < \phi < \psi_2$:

$$\begin{aligned} V_h(\phi) &\approx V_h(\theta) + \tfrac{1}{2}V_h^{(2)}(\theta)(\phi-\theta)^2 + \tfrac{1}{6}V_h^{(3)}(\theta)(\phi-\theta)^3 \\ &\approx V_h(\theta) + \tfrac{1}{6}V_h^{(3)}(\theta^*)(\phi-\theta^*)^3, \end{aligned} \tag{B4}$$

and for $\{\theta_1,\theta_2\}/\phi < \phi < \theta$, we have

$$V_h(\phi) \approx V_h(\psi_1) + \tfrac{1}{6}V_h^{(3)}(\theta^*)(\phi-\theta^*)^3. \tag{B5}$$

From Fig. 20, we can see that we only need to integrate on half of the real line. Hence we have

$$\begin{aligned} \tau &\approx \frac{\delta}{\epsilon}\exp\left[\frac{V_h(\theta)-V_h(\psi_1)}{\epsilon}\right] \\ &\quad\times\int_{\theta^*}^{\infty}\exp\left[\frac{1}{6}V_h^{(3)}(\theta^*)(\phi-\theta^*)^3/\epsilon\right]d\phi \\ &\quad\times\int_{-\infty}^{\theta^*}\exp\left[-\frac{1}{6}V_h^{(3)}(\theta^*)(\varphi-\theta^*)^3/\epsilon\right]d\varphi \\ &= \frac{\delta\left(\int_0^{\infty}e^{-x^3/6}dx\right)^2}{\epsilon^{1/3}|V^{(3)}(\theta^*)|^{2/3}}\exp\left(\frac{\Delta V}{\epsilon}\right). \end{aligned} \tag{B6}$$

[1] J. Daughton, Thin Solid Films **216**, 162 (1992).
[2] G. Pinz, Science **282**, 1660 (1998).
[3] W. F. Brown, Jr., Phys. Rev. **130**, 1677 (1963).
[4] X. Wang, H. N. Bertram, and V. L. Safonov, J. Appl. Phys. **92**, 2064 (2002).
[5] R. V. Kohn, M. G. Reznikoff, and E. Vanden-Eijnden, Nonlinear Science (submitted).
[6] R. H. Koch, G. Grinstein, G. A. Keefe, Yu. Lu, P. L. Trouilloud, W. J. Gallagher, and S. S. P. Parkin, Phys. Rev. Lett. **84**, 5419 (2000).
[7] J. Li and J. Shi, Appl. Phys. Lett. **93**, 3821 (2001).
[8] C. J. García-Cervera and W. E, IEEE Trans. Magn. **39**, 1766 (2003).
[9] E. C. Stoner and E. P. Wohlfarth, Philos. Trans. R. Soc. London, Ser. A **240**, 599 (1948).
[10] C. J. García-Cervera, Z. Gimbutas, and W. E, J. Comput. Phys. **184**, 37 (2003).
[11] J. Miltat, G. Albuquerque, and A. Thiaville, in *Topics in Applied Physics*, Spin Dynamics in Confined Magnetic Structures I, edited by B. Hillebrands and K. Ounadjela (Springer, Berlin, 2002), p. 83.
[12] C. W. Gardiner, *Handbooks of Stochastic Methods for Physics, Chemistry and Natural Sciences*, Springer Series in Synergetics 13 (Springer, Berlin, 1983).
[13] B. J. Matkowsky and Z. Schuss, SIAM J. Appl. Math. **22**, 365 (1977).
[14] F. Martinelli, E. Olivieri, and E. Scoppola, J. Stat. Phys. **55**, 477 (1989).
[15] H. Jónsson, G. Mills, and K. W. Jacobsen, in *Classical and Quantum Dynamics in Condensed Phase Simulations*, edited by B. J. Berne, G. Ciccotti, and D. F. Cokder (World Scientific, Singapore, 1998), p. 385.
[16] W. E, W. Ren, and E. Vanden-Eijnden, J. Appl. Phys. **93**, 2275 (2003).